Science Bulletin 67 (2022) 1874–1881

Contents lists available at ScienceDirect

Science Bulletin

journal homepage: www.elsevier.com/locate/scib

Article

Sub-ambient full-color passive radiative cooling under sunlight based on efficient quantum-dot photoluminescence

Xueyang Wang [a,1], Qian Zhang [a,1], Shuaihao Wang [a,1], Chunqi Jin [b,1], Bin Zhu [a,*], Yucong Su [a], Xunyi Dong [a], Jie Liang [a], Zhenda Lu [a], Lin Zhou [a], Wei Li [b,*], Shining Zhu [a], Jia Zhu [a,*]

[a] National Laboratory of Solid State Microstructures, College of Engineering and Applied Sciences, Jiangsu Key Laboratory of Artificial Functional Materials, Collaborative Innovation Center of Advanced Microstructures, Nanjing University, Nanjing 210093, China
[b] GPL Photonics Lab, State Key Laboratory of Applied Optics, Changchun Institute of Optics, Fine Mechanics and Physics, Chinese Academy of Sciences, Changchun 130033, China

ARTICLE INFO

Article history:
Received 8 May 2022
Received in revised form 9 July 2022
Accepted 17 August 2022
Available online 24 August 2022

Keywords:
Radiative cooling
Full-color
Sub-ambient
Quantum-dot photoluminescence
Electrostatic-spinning/inkjet printing approaches

ABSTRACT

Daytime radiative cooling with high solar reflection and mid-infrared emission offers a sustainable way for cooling without energy consumption. However, so far sub-ambient daytime radiative coolers typically possess white/silver color with limited aesthetics and applications. Although various colored radiative cooling designs have been pursued previously, multi-colored daytime radiative cooling to a temperature below ambient has not been realized as the solar thermal effect in the visible range lead to significant thermal load. Here, we demonstrate that photoluminescence (PL) based colored radiative coolers (PCRCs) with high internal quantum efficiency enable sub-ambient full-color cooling. As an example of experimental demonstration, we develop a scalable electrostatic-spinning/inkjet printing approach to realize the sub-ambient multi-colored radiative coolers based on quantum-dot photoluminescence. The unique features of obtained PCRCs are that the quantum dots atop convert the ultraviolet–visible sunlight into emitted light to minimize the solar-heat generation, and cellulose acetate based nanofibers as the underlayer that strongly reflect sunlight and radiate thermal load. As a result, the green, yellow and red colors of PCRCs achieve temperatures of 5.4–2.2 °C below ambient under sunlight (peak solar irradiance >740 W m^{-2}), respectively. With the excellent cooling performance and scalable process, our designed PCRC opens a promising pathway towards colorful applications and scenarios of radiative cooling.

1. Introduction

As traditional cooling systems consume 15% of global electricity and account for 10% of global greenhouse gas emissions, it is desirable to develop passive cooling technologies [1–3]. Recently, daytime radiative cooling, through reflecting most of the sunlight power and simultaneously dissipating heat to outer space in the atmospheric transmission window (8–13 μm) without any energy consumption, has attracted much attention [4,5]. A variety of daytime radiative cooling designs, such as photonic structures [6,7], hybrid metamaterial films [8–10], and porous polymer structural materials [11–14], have been demonstrated. However, so far sub-ambient daytime radiative coolers under direct sunlight (the averaged peak solar irradiance of midday is above 700 W m^{-2} in the hot regions on Earth) [15–19], only possess white or silver colors. This is because so far only white or silver colors can have reflection above 90% across the solar spectrum (R_{solar} > 0.9) [6,20], one of the key requirements for sub-ambient cooling. As we know, while the white or silver colors based radiative cooling can have various applications, they also have aesthetic and functional limitations, and might cause potential health issues for human eyes [21,22].

It is therefore ideal to pursue colored radiative coolers with a wide color gamut and chroma, while still maintaining superior sub-ambient cooling performance. However, despite significant effort on the designs of colored radiative coolers based on chemical absorbers (pigments, dyes, etc.) [23,24], photonic structures [25–32], and photoluminescent materials [33–38], it is very challenging to achieve the sunlight reflectivity above 0.9, because showing the desired color leads to the inevitable absorption of the visible spectrum (0.4–0.74 μm), and consequential solar thermal effect which increases thermal load.

In this article, we reveal that sub-ambient full-color radiative cooling can be realized through highly efficient photolumines-

* Corresponding authors.
E-mail addresses: binzhu@nju.edu.cn (B. Zhu), weili1@ciomp.ac.cn (W. Li), jiazhu@nju.edu.cn (J. Zhu).
[1] These authors contributed equally to this work.

https://doi.org/10.1016/j.scib.2022.08.028
2095-9273/

cence, which converts the absorbed photons into re-emitted light efficiently, with minimized solar-thermal effect. As an example of experimental demonstration, we report that sub-ambient full-color radiative coolers based on efficient quantum-dot photoluminescence can be achieved through a scalable electrostatic-spinning/inkjet printing method. The obtained PCRC consists of an underlayer made of cellulose acetate (CA) nanofibers film and a top layer containing a colorant of photoluminescent perovskite quantum dots (Fig. 1a–c). Under sunlight illumination, the top layer absorbs and emits visible light of the desired color, while the underlayer maximizes the backscattering of sunlight transmitted by the top layer and radiates heat due to the high mid-infrared emission (Fig. 1d). More importantly, we achieve multicolor patterned PCRCs at large scale (Fig. 1c), combining scalable roll-to-roll electrospinning to synthesize the CA nanofibers (Fig. 1a), with the commercialized inkjet printing to coat the perovskite quantum dots with high quantum efficiency on the CA nanofibers (Fig. 1b).

2. Materials and methods

2.1. Preparation of the PCRCs

2.1.1. Preparation of perovskite quantum dots $CsPbX_3$ (X = Br, I)

Firstly, 0.407 g Cs_2CO_3, 20 mL octadecne (ODE), and 1.5 mL oleic acid were mixed in a 50 mL three-necked flask and heated to 120 °C under the protection of N_2 and kept for 20 min to form cesium oleate. Secondly, octadecene (10 mL), oleamine (2 mL), oleic acid (1 mL) and PbX_2 (0.376 mmol) (the specific proportion depends on the color of the sample required, such as green: $PbBr_2$ (0.13 g); yellow: $PbBr_2$ (0.084 g), PbI_2 (0.07 g); red: $PbBr_2$ (0.0414 g), PbI_2 (0.1218 g)), were added to a 50 mL three-necked flask and heated to 120 °C under the protection of N_2 for 20 min to completely dissolve PbX_2. Then heated to 150 °C for 5 s, 1 mL of the above cesium oleate solution was quickly added and cooled in an ice bath to form $CsPbX_3$. Lastly, the cooled solution was centrifuged after adding ethanol or acetone with a volume ratio of 1:1. After centrifugation, the supernatant was poured out and the precipitation ($CsPbX_3$) was dissolved in cyclohexane for later use.

2.1.2. Preparation of CA/$CsPbX_3$ film

The CA fibrous network was fabricated via electrospinning. Acetone and dimethyl formamide (DMF) were mixed with a volume ratio of 1:4. Then 17 wt% of CA powder was dissolved in the mixture. The electrospinning was done with a tip-to-collector distance of 15 cm, a voltage difference of ~18 kV, and a mass flow rate of 0.4 mL h^{-1}. The prepared $CsPbX_3$ suspension (0.00887 g mL^{-1}) was sprayed onto CA film surfaces. The amount of sprayed solution is 1.5 mL cm^{-2}. Finally, a hydrophobic agent (1*H*, 1*H*, 2*H*, 2*H*-perfluorooctyltrichloro) was sprayed onto CA/$CsPbX_3$ film to form the PCRC.

2.2. Material characterizations of the PCRCs

The micro-images of the PCRC were captured by scanning electron microscopy (SEM, MIRA3, TESCAN). The photoluminescence quantum yield of PCRCs was investigated by (Steady-state transient fluorescence spectrometer FLS980 Attenborough). A UV–vis–NIR spectrophotometer (UV-360, SHIMADZU) equipped with an integrating sphere (ISR-310) was used to measure the sunlight reflectivity spectrum of samples. The mid-infrared emissivity spectrum and Fourier transform infrared spectra of PCRC/CA nanofibers film were measured with a Fourier transform infrared (FTIR) spectrophotometer (Nicolet iS50R, Thermo Fisher) equipped with an integrating sphere (4P-GPS-020-SL, Pike).

2.3. Cooling performances of the PCRCs

The PCRC temperature was monitored by K-type thermocouples. The cooling power was obtained by monitoring the heating power of the Kapton heater by a power meter (66205, Chroma). The heating load with a constant power was applied by the Kapton heater with a temperature feedback circuit. The temperature feedback circuit heats the colored radiative cooler to the ambient temperature. And the measured heating power is the compensated cooling power. The sunlight power was measured by a solar radiation meter (TBQ) or a portable solar power meter (1333R, TES). The ambient temperature and relative humidity were monitored by a temperature and humidity recorder in a shelter (Tuolaisi Co., ltd.). The infrared images were taken using an infrared camera (Fluke tix580).

3. Results and discussion

In order to achieve sub-ambient cooling for a PCRC, one must consider the radiative thermal load of a PCRC with a specific color from a perspective of energy balance. Fig. 1e shows the ideal spectrum for a PCRC that can absorb and emit light. The net radiative thermal load of the PCRC in general can be written as:

$$P_{\text{net}} = P_{\text{sun}}^{\text{visible}} + P_{\text{sun}}^{\text{infrared}} - P_{\text{cooling}}. \quad (1)$$

P_{cooling} is the net radiative cooling power in the absence of sunlight. As calculated by Rephaeli et al. [20], the maximum power for radiative cooling is about 150 W m^{-2} at 298 K. $P_{\text{sun}}^{\text{infrared}}$ is the absorbed power density from the infrared part of the solar spectrum (0.7 to 2.5 μm), which is 453 W m^{-2} for AM 1.5 spectrum. $P_{\text{sun}}^{\text{visible}}$ is the net absorbed power from the visible and ultraviolet part of the solar spectrum (0.28 to 0.7 μm).

For the PCRC, in addition to absorption in specific visible and ultraviolet bands, some of the absorbed energy is re-emitted in visible light. So, the net absorption of visible light is the absorbed energy ($P_{\text{absorption}}^{\text{visible}}$) minus the emitted energy ($P_{\text{emssion}}^{\text{visible}}$). η is the total energy conversion efficiency of photons which is derived from the PL internal quantum yield (more calculations can be found in Supplementary materials Note 1).

$$P_{\text{sun}}^{\text{visible}} = P_{\text{absorption}}^{\text{visible}} - P_{\text{emission}}^{\text{visible}}, \quad (2)$$

$$P_{\text{emission}}^{\text{visible}} = \eta P_{\text{absorption}}^{\text{visible}}. \quad (3)$$

Therefore, combining all three terms in Eq. (1) as discussed above, we can see that in principle PCRC can possess the same color but significantly different net radiative thermal loads due to different internal quantum efficiencies. We calculate the tunable range of thermal loads for all colors of PCRC under sunlight by using Eq. (1) and exploring the metamerism effect (Supplementary materials Note 1 for more details). Fig. 1f shows the tunable range of thermal loads as the colors change from purple to red, with the lightness L = 60, saturation C_{ab} = 60, and hue angle h_{ab} = arctan (b/a) from 360° to 0°. It is noted that the thermal loads of the green, blue and red PCRCs can be below zero (corresponding to sub-ambient cooling), only when the PL internal quantum yields of PCRCs are above 0.73, 0.62, and 0.80, respectively (Fig. S1 online).

We also carried out the study over the entire color space (Fig. S2 online) with all other colors. The minimum radiative thermal loads of all PCRCs can be less than zero, which means all colors can achieve net cooling power based on the high photon conversion efficiency. Based on the thermal load of PCRCs, the cooling temperature of colored surfaces under typical outdoor conditions was studied by balancing P_{net} with non-radiative heat loss $P_{\text{cond+conv}} = h_c(T - T_{\text{amb}})$, where h_c is the non-radiative heat

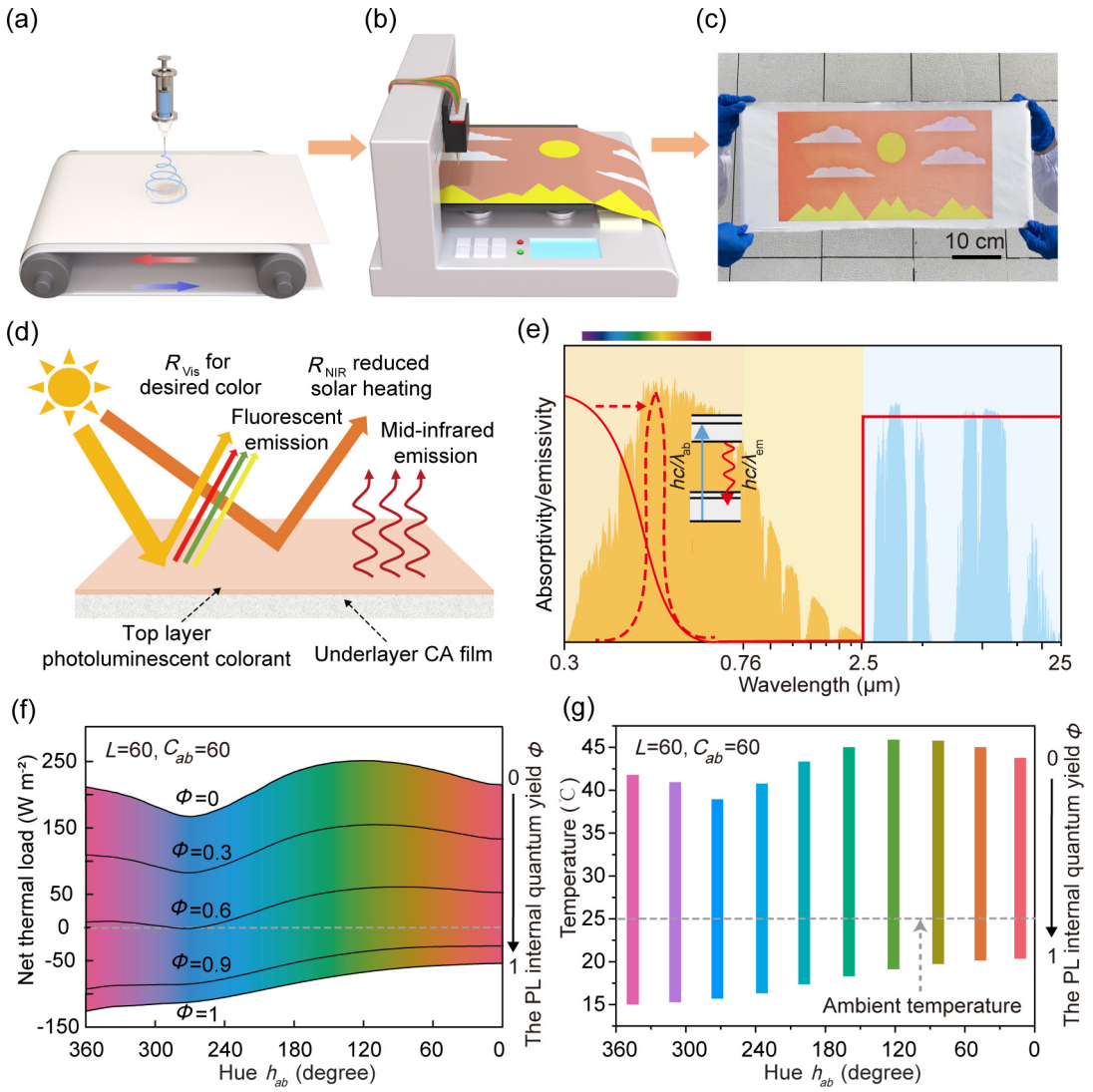

Fig. 1. Fabrication, structure, and mechanism of PCRC. (a) Schematic of the electrostatic-spinning setup for producing CA nanofibers film. (b) Schematic of the process for inkjet printing with photoluminescence colorants. (c) The photograph of multicolor PCRC with sunrise using electrostatic-spinning/inkjet printing. (d) Schematic of the bilayer PCRC design that consists of the photoluminescent colorant (perovskite quantum dots) and CA nanofibers film. The photoluminescent colorant absorbs and emits visible wavelengths to achieve the desired color. The CA nanofibers film reflects any sunlight transmitted by the top layer and radiates energy out. (e) The ideal absorptivity/emissivity spectra of PCRCs. AM 1.5 G solar spectrum (orange shaded area), and atmosphere transmittance (light blue shaded area) are plotted for references. (f) Tunable net thermal load of PCRCs with fixed lightness (L = 60), saturation (C_{ab} = 60), and hue angle (h_{ab} = arctan(b/a) from 360° to 0°), as a function of the PL internal quantum yield (from 0 to 1). (g) Tunable temperature range of common colors under a typical non-radiative heat dissipation condition h_c = 12 W m^{-2} K^{-1}, as a function of the PL internal quantum yield (from 0 to 1).

coefficient considering both conduction and convection. In this calculation, we assumed a typical h_c = 12 W m^{-2} K^{-1} (1 m s^{-1} wind speed), T_{amb} = 25 °C. Fig. 1g shows the cooling temperatures of most common colors. For example, the green PCRC can achieve a maximum of ~7.7 °C below ambient temperature, in contrast to the fact that a conventional green cooler typically reaches 44 °C (19 °C above the ambient temperature) even with consideration of metamerism, near-infrared solar absorption, and radiative cooling [25] in an outdoor environment under sunlight. Our theoretical results indicate that the high photon conversion efficiency is vital for achieving sub-ambient cooling of all the PCRCs.

As an example of demonstration to realize sub-ambient cooling, $CsPbX_3$ quantum dots were chosen as photoluminescent colorants due to their high-quantum-yield photoluminescence [39,40]. We developed three primary colors of green, yellow, and red PCRCs by adjusting the cesium lead halide quantum dots composition through the scalable manufacturing process above [41] (details of the $CsPbX_3$ quantum dots synthesis are given in the methods section and Fig. S3 online). However, to fully realize the potential high photon conversion efficiency of $CsPbX_3$ quantum dots in the obtained PCRCs, there are several fundamental challenges that need to be overcome. First of all, the $CsPbX_3$ quantum dots are not stable in the air, severely diminishing the photon conversion performance [42–44]. Secondly, the $CsPbX_3$ quantum dots can easily agglomerate to compromise their quantum efficiency [45]. Here, we synthesized CA film of randomly stacked nanofibers with diameter sizes broadly distributed as the underlayer through electrostatic spinning, to strongly scatter sunlight (Fig. 2a). Then we coated $CsPbX_3$ quantum dots on the CA film through a scalable inkjet printing method, which enable uniform distribution of $CsPbX_3$ without obvious agglomeration (Fig. 2b). A hydrophobic layer (1*H*, 1*H*, 2*H*, 2*H*-perfluorooctyltrichloro) was subsequently sprayed on the CA/$CsPbX_3$ film to isolate water molecules in the air (Fig. 2c), stabilizing the $CsPbX_3$ quantum dots. Moreover, it is

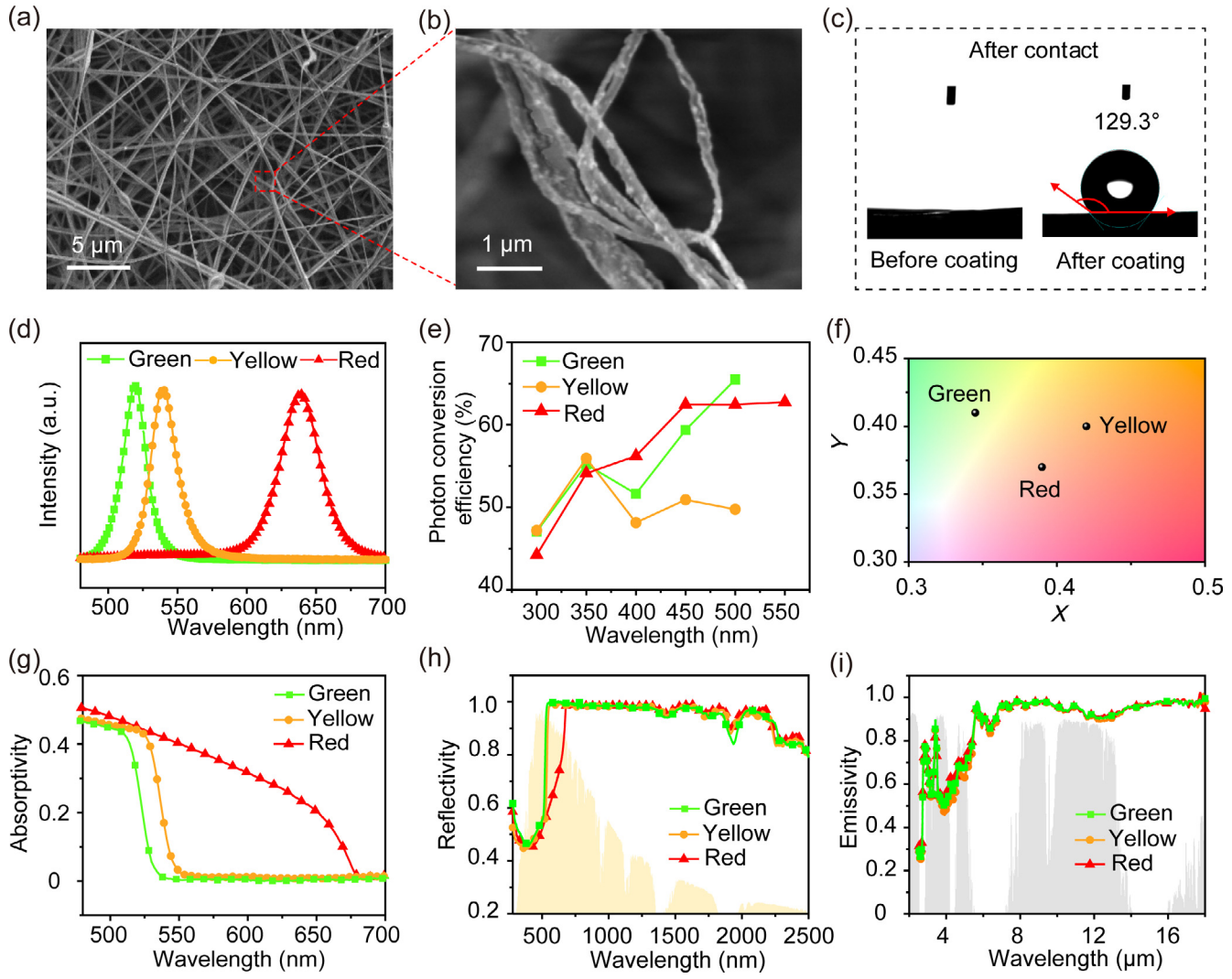

Fig. 2. Structural and optical characterizations of the PCRC. (a) High-magnification scanning electron microscopy (SEM) image of the PCRC. (b) The high-resolution SEM image of CA/$CsPbX_3$ fibers. The $CsPbX_3$ quantum dots are evenly distributed on the surface of the CA fibers. (c) Contact angles of CA/$CsPbX_3$ before coating hydrophobic layer (left) and after coating hydrophobic layer (right). It clearly suggests that CA/$CsPbX_3$ before coating hydrophobic layer is hydrophilic, as it only takes 1 s for water drop to infiltrate into surface, while CA/$CsPbX_3$ after coating hydrophobic layer becomes hydrophobic. (d) The steady-state photoluminescence spectra of the green, yellow, and red PCRCs. (e) Photon conversion efficiencies of the green, yellow, and red PCRCs. (f) The chromaticity of the green, yellow, and red PCRCs shown in the CIE 1931 color space. (g) The visible sunlight absorptivity spectra of the green, yellow, and red PCRCs. (h) The sunlight reflectivity spectra of the green, yellow, and red PCRCs. (i) The mid-infrared emissivity spectrums of the green, yellow, and red PCRCs.

noteworthy that O-Pb bonding can be formed between the CA and $CsPbX_3$ (Fig. S4 online) [45–48], further increasing the stability of $CsPbX_3$ quantum dots.

To examine the optical performance of the obtained CA/$CsPbX_3$ PCRCs, we carried out the PL test of PCRCs. It shows that the peaks of green, yellow and red PCRCs are 520, 540, and 650 nm, corresponding to the cutoff wavelengths of absorption (Fig. 2d and g). To quantitatively measure the conversion efficiency of PCRCs from absorbed light energy to emitted light, we calculated the photon conversion efficiency for each color of PCRC by measuring the PL internal quantum yield. The average PL internal quantum yield of green, yellow, and red PCRCs is 0.73, 0.68, and 0.83, respectively (more details about calculations can be found in Supplementary materials Note 2 and Figs. S5–S8 online). The calculated photon conversion efficiencies of green, yellow, and red PCRCs are ~ above 50%, as shown in Fig. 2e. In other words, >50% of the absorbed sunlight energy is emitted in the visible desired color band, which greatly reduces the solar-heat generation and enables sub-ambient cooling performance under sunlight.

The positions of the green, yellow and red PCRCs in the CIE 1931 color diagram disclose the differences in color properties (Fig. 2f). The solar reflection spectra of PCRCs show high reflectivity (mostly above 90%) in other solar wavelength ranges except for visible absorption for desired colors (Fig. 2h). The weighted reflectivity of green, yellow and red PCRCs for the solar spectrum (0.28–2.5 μm) are 0.89, 0.87, and 0.82, respectively (the weighted reflectivity of the single CA film is 0.975, Fig. S9 online). Combining with their high photon conversion efficiencies above, the equivalent effective reflectivity of green, yellow and red PCRCs are all higher than 0.9. The mid-infrared emissivity spectrum in Fig. 2i verifies that the obtained PCRCs also possess an average high mid-infrared emissivity of 0.95 in the atmospheric transparent window (8–13 μm). Consequently, the high solar reflectivity and mid-infrared emissivity of the obtained PCRC lay a solid foundation for achieving sub-ambient radiative cooling.

To experimentally verify the passive radiative cooling performance of the PCRCs, we performed an outdoor temperature measurement via the setups shown in Fig. 3a and b. Here, the white

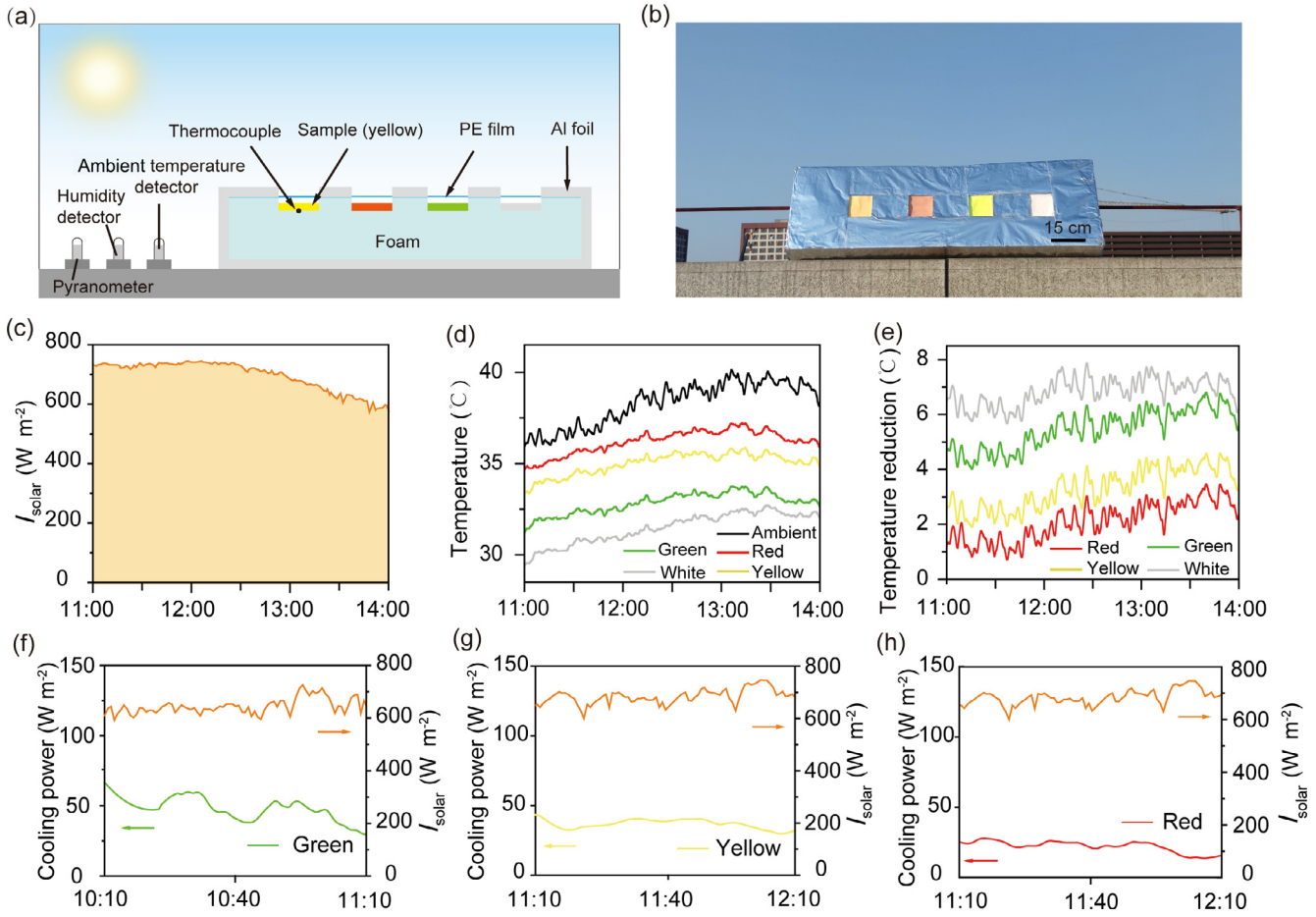

Fig. 3. Sub-ambient cooling performance of the PCRCs. (a) The sectional schematic of the experimental setup used to test the cooling performance. The PE film and foam are used to minimize the impact of the surroundings. (b) The photograph of the setup of the PCRCs' cooling performance tests in a clear day. (c) The power of incident sunlight and (d) temperature profiles of the green, yellow, and red PCRCs in Nanjing, China (32°3′25.02″N, 118°46′44.36″E, October 3, 2021). (e) Temperature reductions of the green, yellow, and red PCRCs ($T_{ambient} - T_{sample}$). (f)–(h) Power of incident sunlight and the cooling power of the green, yellow, and red PCRCs in Nanjing, China (32°3′25.02″N, 118°46′44.36″E, November 16, 2021).

radiative cooler is set as the control group. In Fig. 3c–e, we monitored the temperature profiles of the green, yellow, and red PCRCs via thermocouples on a clear day with peak solar irradiance >740 W m^{-2} (the averaged peak solar irradiance of midday is above 700 W m^{-2} in the hot regions on Earth [15–19]) and an averaged ambient temperature of ~37.5 °C (the humidity during measurement is shown in Fig. S10 online). Sub-ambient temperature ($T_{ambient} - T_{sample}$) is an important indicator to evaluate the cooling performance of a radiative cooler. It is observed that the green, yellow and red PCRCs enable mean sub-ambient cooling temperatures of ~5.4, ~3.4, and ~2.2 °C, respectively (Fig. 3d, e). Notably, the excellent sub-ambient cooling performance of the PCRCs is stable over a long period of time, as shown in Figs. S11–S13 (online). To further evaluate the radiative cooling performance, we subsequently monitored the cooling power at ambient temperature for all PCRCs, The cooling power of green, yellow, and red PCRCs are ~51.7, ~36.9, and ~25.6 W m^{-2} with peak solar irradiance >720 W m^{-2} (Fig. 3f–h) and at an ambient temperature/relative humidity of ~18 °C/40% (the ambient temperature/humidity during measurement are shown in Fig. S14 online). Moreover, we performed a comparison between the radiative cooling performance of our fabricated PCRCs and the previously reported colored radiative coolers (Table S1 online). All these results consistently confirm that our designed PCRC stands out as a high performing colored radiative cooling material during the daytime.

It is noteworthy that our designed PCRCs can be realized on different matrix materials through the inkjet printing process, which is crucial for practical applications. As an experimental demonstration, we print the emblem of Nanjing University on various flexible white radiative cooling substrates like CA film, cotton, and polyvinylidene fluoride (PVDF) film (Fig. 4a–d). Colored radiative cooling devices can be widely applied for cooling buildings, outdoor facilities, and personal devices. Here we examine the cooling performance of the designed PCRC as an outdoor colorful tent. We observed a temperature reduction of ~4 °C for the PCRC based tent, compared to a commercial tent with the same color, under a mean sunlight intensity of ~800 W m^{-2} (Fig. 4e, f; the ambient conditions during measurements are presented in Fig. S15 online and the solar reflectivity spectrum of the commercial tent is shown in Fig. S16 online). Fig. 4g presents the infrared images of the commercial tent and PCRC based tent with the same color under a clear sky during 20 min in Nanjing, China (see Fig. S17 online for detailed meteorological information). The images show that the temperature of the PCRC tent stays lower than that of the commercial tent. In addition, PCRC paints can be used on building paints. As shown in Fig. S18 (online), PCRC paints can achieve almost the same color as commercial paints. And under direct sunlight (700 W m^{-2}), the temperatures of PCRC paints are 2.2–4.6 °C lower than conventional paints. It further illustrates the superior cooling ability of our proposed PCRCs under practical conditions.

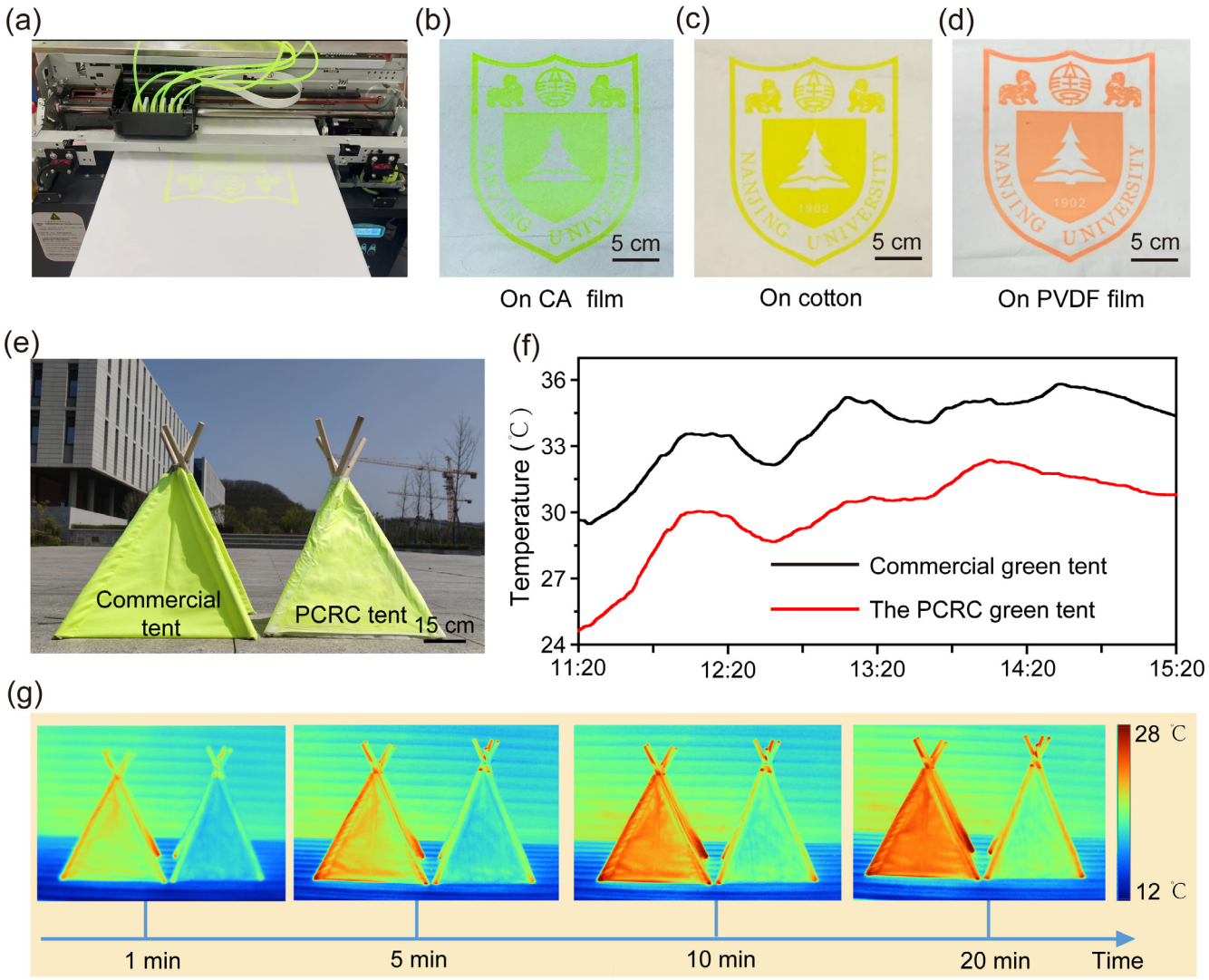

Fig. 4. Potential applications of the PCRCs. (a) The Photograph of the PCRC fabric during inkjet printing. (b–d) Optical photographs of PCRC fabric with the emblem of Nanjing University using inkjet printing, including green (b), yellow (c), and red (d). (e) Photograph of PCRC based green tent and commercial green tent. (f) Temperature variation of a commercial green tent and a PCRC based green tent, running the same application under the same environmental conditions in Nanjing, China (32°3′25.02″N, 118°46′44.36″E, March 15, 2022). (g) Infrared images of a commercial green tent and a PCRC based green tent under sunlight (800 W m^{-2}) (32°3′25.02″N, 118°46′44.36″E, March 24, 2022).

4. Conclusion

In summary, we demonstrate the colored radiative cooling based on efficient photoluminescence with sub-ambient full-color radiative cooling performance. Through a scalable electrostatic-spinning/inkjet printing process, which leads to versatile compatibility, the PCRCs can be integrated into various products for different scenarios, such as tents and flexible color patterned fabrics. It is expected that this superior cooling performance, vivid colors together with scalable processes will greatly expand the application scenarios of passive radiative cooling.

Conflict of interest

The authors declare that they have no conflict of interest.

Acknowledgments

We acknowledge the micro-fabrication center at the National Laboratory of Solid State Microstructures (NLSSM) for technical support. This work was jointly supported by the National Key Research and Development Program of China (2021YFA1400700, 2020YFA0406104, and 2017YFA0205700), the National Natural Science Foundation of China (52002168, 12022403, 11874211, 61735008, 62134009, and 62121005), Science Foundation of Jiangsu (BK20190311), Key Science and Technology Innovation Programme of Shandong Province (2019JZZY020704), Excellent Research Programme of Nanjing University (ZYJH005), and the Fundamental Research Funds for the Central Universities (021314380214, 021314380190, 021314380140, and 021314380150). J.Z. acknowledges support from the XPLORER PRIZE.

Author contributions

Jia Zhu, Bin Zhu, and Xueyang Wang conceived and planned this research. Xueyang Wang, Shuaihao Wang, and Qian Zhang, Yucong Su, Xunyi Dong, and Jie Liang did the experiments. Wei Li and Chunqi Jin contributed to the optical modeling and thermal analysis. Xueyang Wang, Shuaihao Wang, Bin Zhu, Zhenda Lu, Wei Li, Lin Zhou, Shining Zhu, and Jia Zhu organized the data and wrote the manuscript. All authors discussed the results and approved the final version of the manuscript.

Appendix A. Supplementary materials

Supplementary materials to this article can be found online at https://doi.org/10.1016/j.scib.2022.08.028.

References

[1] Fleischer AS. Cooling our insatiable demand for data. Science 2020;370:783–4.
[2] Biardeau LT, Davis LW, Gertler P, et al. Heat exposure and global air conditioning. Nat Sustain 2020;3:25–8.
[3] Isaac M, Van Vuuren DP. Modeling global residential sector energy demand for heating and air conditioning in the context of climate change. Energy Policy 2009;37:507–21.
[4] Zhang Q, Wang S, Wang X, et al. Recent progress in daytime radiative cooling: advanced material designs and applications. Small Methods 2022;6:2101379.
[5] Fan S, Li W. Photonics and thermodynamics concepts in radiative cooling. Nat Photonics 2022;16:182–90.
[6] Raman AP, Anoma MA, Zhu L, et al. Passive radiative cooling below ambient air temperature under direct sunlight. Nature 2014;515:540–4.
[7] Zhang H, Ly KC, Liu X, et al. Biologically inspired flexible photonic films for efficient passive radiative cooling. Proc Natl Acad Sci USA 2020;117:14657–66.
[8] Zhai Y, Ma Y, David SN, et al. Scalable-manufactured randomized glass-polymer hybrid metamaterial for daytime radiative cooling. Science 2017;355:1062–6.
[9] Zeng S, Pian S, Su M, et al. Hierarchical-morphology metafabric for scalable passive daytime radiative cooling. Science 2021;373:692–6.
[10] Zhu B, Li W, Zhang Q, et al. Subambient daytime radiative cooling textile based on nanoprocessed silk. Nat Nanotechnol 2021;16:1342–8.
[11] Mandal J, Fu Y, Overvig AC, et al. Hierarchically porous polymer coatings for highly efficient passive daytime radiative cooling. Science 2018;362:315–9.
[12] Li D, Liu X, Li W, et al. Scalable and hierarchically designed polymer film as a selective thermal emitter for high-performance all-day radiative cooling. Nat Nanotechnol 2021;16:153–8.
[13] Hsu P-C, Song AY, Catrysse PB, et al. Radiative human body cooling by nanoporous polyethylene textile. Science 2016;353:1019–23.
[14] Li T, Zhai Y, He S, et al. A radiative cooling structural material. Science 2019;364:760–3.
[15] Alshahrani A, Omer S, Su Y. An investigation into the potential of hosting capacity and the frequency stability of a regional grid with increasing penetration level of large-scale PV systems. Electronics 2021;10:1254.
[16] Samy A, Shaffie A, Aly H. Comparative and evaluate of empirical models for estimation global solar radiation in Al-Baha, KSA. J Earth Sci Clim Change 2018;9:1000492.
[17] Babikir MH, Njomo D, Khayal MY, et al. Estimation of direct solar radiation of chad. Energy Power Eng 2018;10:212–25.
[18] Al-Aboosi FY. Models and hierarchical methodologies for evaluating solar energy availability under different sky conditions toward enhancing concentrating solar collectors use: Texas as a case study. Int J Energy Environ Eng 2020;11:177–205.
[19] Garg H. Solar energy: fundamentals and applications. Tata McGraw-Hill Education; 2000.
[20] Rephaeli E, Raman A, Fan S. Ultrabroadband photonic structures to achieve high-performance daytime radiative cooling. Nano Lett 2013;13:1457–61.
[21] Lozano LM, Hong S, Huang Y, et al. Optical engineering of polymer materials and composites for simultaneous color and thermal management. Opt Mater Express 2019;9:1990–2005.
[22] Synnefa A, Santamouris M, Apostolakis K. On the development, optical properties and thermal performance of cool colored coatings for the urban environment. Sol Energy 2007;81:488–97.
[23] Chen Y, Mandal J, Li W, et al. Colored and paintable bilayer coatings with high solar-infrared reflectance for efficient cooling. Sci Adv 2020;6:eaaz5413.
[24] Cai L, Peng Y, Xu J, et al. Temperature regulation in colored infrared-transparent polyethylene textiles. Joule 2019;3:1478–86.
[25] Li W, Shi Y, Chen Z, et al. Photonic thermal management of coloured objects. Nat Commun 2018;9:1–8.
[26] Lee GJ, Kim YJ, Kim HM, et al. Colored, daytime radiative coolers with thin-film resonators for aesthetic purposes. Adv Opt Mater 2018;6:1800707.
[27] Sheng C, An Y, Du J, et al. Colored radiative cooler under optical tamm resonance. ACS Photonics 2019;6:2545–52.
[28] Cho J-W, Lee E-J, Kim S-K. Full-color solar-heat-resistant films based on nanometer optical coatings. Nano Lett 2022;22:380–8.
[29] Yalçın RA, Blandre E, Joulain K, et al. Colored radiative cooling coatings with nanoparticles. ACS Photon 2020;7:1312–22.
[30] Kim HH, Im E, Lee S. Colloidal photonic assemblies for colorful radiative cooling. Langmuir 2020;36:6589–96.
[31] Ding Z, Pattelli L, Xu H, et al. Iridescent daytime radiative cooling with no absorption peaks in the visible range. Small 2022;18:2202400.
[32] Shanker R, Ravi Anusuyadevi P, Gamage S, et al. Structurally colored cellulose nanocrystal films as transreflective radiative coolers. ACS Nano 2022;16:10156–62.
[33] Yoon TY, Son S, Min S, et al. Colloidal deposition of colored daytime radiative cooling films using nanoparticle-based inks. Mater Today Phys 2021;21:100510.
[34] Jeon S, Son S, Lee SY, et al. Multifunctional daytime radiative cooling devices with simultaneous light-emitting and radiative cooling functional layers. ACS Appl Mater Interfaces 2020;12:54763–72.
[35] Min S, Jeon S, Yun K, et al. All-color sub-ambient radiative cooling based on photoluminescence. ACS Photon 2022;9:1196–205.
[36] Yalçın RA, Blandre E, Joulain K, et al. Colored radiative cooling coatings with fluorescence. J Photonics Energy 2021;11:032104.
[37] Son S, Jeon S, Chae D, et al. Colored emitters with silica-embedded perovskite nanocrystals for efficient daytime radiative cooling. Nano Energy 2021;79:105461.
[38] Son S, Jeon S, Bae J, et al. Efficient radiative cooling emitter adopting the wavelength conversion of giant CdSe/ZnS core-shell nanocrystals. Mater Today Phys 2021;21:100496.
[39] Chen D, Liu Y, Yang C, et al. Promoting photoluminescence quantum yields of glass-stabilized $CsPbX_3$ (X= Cl, Br, I) perovskite quantum dots through fluorine doping. Nanoscale 2019;11:17216–21.
[40] Song J, Li J, Li X, et al. Quantum dot light-emitting diodes based on inorganic perovskite cesium lead halides ($CsPbX_3$). Adv Mater 2015;27:7162–7.
[41] Kovalenko MV, Protesescu L, Bodnarchuk MI. Properties and potential optoelectronic applications of lead halide perovskite nanocrystals. Science 2017;358:745–50.
[42] Dai J, Wu Y, Jia R, et al. Strategies of improving $CsPbX_3$ perovskite quantum dots optical performance. Front Mater 2022;9:845977.
[43] Thapa S, Bhardwaj K, Basel S, et al. Long-term ambient air-stable cubic $CsPbX_3$ perovskite quantum dots using molecular bromine. Nanoscale Adv 2019;1:3388–91.
[44] Raja SN, Bekenstein Y, Koc MA, et al. Encapsulation of perovskite nanocrystals into macroscale polymer matrices: enhanced stability and polarization. ACS Appl Mater Interfaces 2016;8:35523–33.
[45] Xue J, Wang R, Yang Y. The surface of halide perovskites from nano to bulk. Nat Rev Mater 2020;5:809–27.
[46] Mei S, Yang B, Wei X, et al. Facile synthesis and optical properties of $CsPbX_3$/ZIF-8 composites for wide-color-gamut display. Nanomaterials 2019;9:832.
[47] Ali I, Peng C, Lin D, et al. Encapsulated green magnetic nanoparticles for the removal of toxic Pb^{2+} and Cd^{2+} from water: development, characterization and application. J Environ Manage 2019;234:273–89.
[48] Chen H, Guo A, Zhu J, et al. Tunable photoluminescence of $CsPbBr_3$ perovskite quantum dots for their physical research. Appl Surf Sci 2019;465:656–64.

Xueyang Wang received her Bachelor's degree from Nanjing University of Science and Technology (2017). Now, she is working as a Ph.D. student in Prof. Zhu's group at the Department of Materials Science and Engineering, Nanjing University. Her research interest focuses on radiative cooling and solar-thermal water treatment.

Qian Zhang is currently a postdoctoral research fellow at Nanjing University. He received his Master's degree at Wuhan Textile University and earned his Ph.D. degree at Hubei University. His research focuses on radiative cooling, photothermal manipulation, and functional fabric.

Shuaihao Wang obtained her Bachelor's degree from Nanjing University in 2019. Now, he is working as a master student in Prof. Zhu's group at the Department of Materials Science and Engineering, Nanjing University. Her research interest focuses on radiative cooling.

Chunqi Jin received her Bachelor's degree from Changchun University of Science and Technology (2014). She studied in Prof. Thomas Pertsch's group at Friedrich Schiller University Jena as an exchange Ph.D. student (2016–2017). She received her Ph.D. degree from University of Chinese Academy of Sciences (UCAS) (2019). She was a postdoctoral fellow at Tsinghua University. She is now an assistant professor at Changchun Institute of Optics, Fine Mechanics and Physics (CIOMP), Chinese Academy of Sciences (CAS). Her research interest focuses on the design and applications of metasurfaces including metalens and multi-dimensional light field detection.

Bin Zhu received his B.S. degree in Materials Physics from Nanjing University in 2013 and his Ph.D. degree in Materials Science and Engineering from Nanjing University in 2018. He became an associate professor at Nanjing University from 2021. His research interest includes thermal management and radiative cooling.

Wei Li received his Bachelor's degree from the Honors School at Harbin Institute of Technology (2011) and his Ph.D. degree from Vanderbilt University (2016). He was a postdoctoral fellow at Stanford University, working with Prof. Shanhui Fan. He is now a professor at Changchun Institute of Optics, Fine Mechanics and Physics (CIOMP), Chinese Academy of Sciences (CAS). He also serves as the director of GPL Photonics Laboratory at CIOMP. His research interest focuses on thermal photonics and energy applications including radiative cooling and solar energy harvesting.

Jia Zhu received his B.S. degree in Physics from Nanjing University in 2003 and his M.S. and Ph.D. degrees in Electrical Engineering from Stanford University in 2006 and 2010 respectively. He went on to work as a postdoctoral scholar at the University of California, Berkeley. In 2013, he became a professor in the College of Engineering and Applied Sciences at Nanjing University. He leads a group of researchers working on nanomaterials for energy conversion and storage.